TURBULENCE STRUCTURE AND TRANSPORT MECHANISM IN A HOMOGENEOUS SHEAR FLOW (REYNOLDS NUMBER EFFECTS)

M. Iwatsuki, O. Iida and Y. Nagano
Department of Mechanical Engineering,
Nagoya Institute of Technology,
Gokiso-cho, Showa-ku, Nagoya 466-8555, Japan

ABSTRACT

Direct numerical simulations (DNS) are carried out to investigate the kinematics of vortical structures in a homogeneous shear flow. Generated longitudinal (streamwise) vortices are conditionally averaged over all the computational region. The effects of the non-linear term on their kinematics are investigated by comparing the DNS and Rapid Distortion Theory (RDT) in both high and low Reynolds number flow fields. It is found that the strain rates in the vortical structure are generated by the effects of the non-linear term and closely associated with the kinematics of the vortical structure. As the Reynolds number increases, the wrapping of the streamwise velocity fluctuation around the vortex is more enhanced to augment the strain rate inside the vortex.

INTRODUCTION

In engineering flow problems, a turbulent shear flow is one of the common subjects. Especially, the inner region of wall turbulence, which has a large shear rate, has been the subject of many investigations. By accumulated experimental and numerical studies on wall-bounded turbulent shear flows, it is confirmed that there exist the quasi-coherent streamwise vortices (Kline et al., 1967; Robinson, 1991). They are elongated in the streamwise direction and found to play an important role in generating the Reynolds stresses and their redistribution (Robinson, 1991; Iida and Nagano, 1998). Thus, the detailed study on the streamwise vortices should give a useful insight into how to construct a structure-based turbulence model, and provide a rational control strategy of turbulence.

A homogeneous shear flow has often been used to study the effects of a mean shear on turbulence because there is no solid boundary to suppress the velocity fluctuations and the effects of the mean shear are more marked (Rogers and Moin, 1987; Lee et al., 1990; Kida and Tanaka, 1994; Matsumoto et al., 1994). Lee et al. (1990) have performed the DNS of a homogeneous shear flow with the shear-rate parameter almost equal to a value at $y^+ = 10$ in a wall shear flow, and show that the low- and high-speed streaks are generated as in wall turbulence. Hence, the high shear rate alone sufficiently generates the structures characteristic of near-wall turbulence. The rapid distortion theory (RDT) neglecting the non-linear term, is found to predict the streaky structure (Lee et al., 1990). Matsumoto et al. (1994) have also found that by comparing the DNS and RDT results of a homogeneous shear flow, no apparent difference is observed in the Reynolds shear stresses and their budgets.

On the other hand, it should be equally of great importance to investigate the effects of the non-linear term. Kida and Tanaka (1994) showed that when a mean shear is imposed on homogeneous isotropic turbulence, the blob-like vortical structures are elongated in the streamwise direction to become the longitudinal vortices. It was also found that the streamwise vortex generates a spanwise vorticity layer, which finally rolls up into the vortex tubes via the Kelvin-Helmholz instability. Hence, they demonstrated some effects of the non-linear term on the longitudinal vortical structures in a homogeneous shear flow. Rogers and Moin (1987) have studied the structure of vortices in homogeneous shear flows of both high and low Reynolds numbers. In their study, the presence of hairpin vortices is ascertained in both cases of Reynolds numbers. Moreover, they also discussed the effect of the Reynolds number

on the average spacing between the leg of the hairpin vortices.

In this study, first the kinematics of the longitudinal vortical structures is investigated to clarify the essential roles of the non-linear term by comparing DNS and RDT at a relatively low Reynolds number. Then, the numerical simulation of the higher Reynolds number is carried out and the effects of the Reynolds number are studied on the kinematics of the vortices. As a result, some similarities are found in the vortical structure between the homogeneous shear flow at a low Reynolds number and the turbulent channel flow. It is also found that the effects of the Reynolds number are more clearly observed in the vortex-stretching inside the streamwise vortex.

RESULTS AND DISCUSSION

We performed both DNS and RDT analyses of a homogeneous shear flow at low Reynolds number with grid points of $64 \times 64 \times 64$ in the streamwise(x_1), normal(x_2) and spanwise(x_3) directions, respectively. The case of relatively higher Reynolds number is numerically simulated with 128^3 grid points. The mean shear rate is defined as $S = dU_1/dx_2$. In the following, all velocity fluctuations and length scale in this study are non-dimensionalized by $\sqrt{S\nu/2}$ $(= 5\pi/19)$ and $\sqrt{2\nu/S}$ $(= 2\pi/190)$, where ν is the kinematic viscosity. The sizes of the computational region L_1, L_2 and L_3 are $4\pi\sqrt{S/2\nu}(= 380)$, $2\pi\sqrt{S/2\nu}$ and $2\pi\sqrt{S/2\nu}$ in the x_1, x_2 and x_3 directions, respectively. In both DNS and RDT, the same isotropic turbulence is used as the initial condition. The initial Reynolds number $Re_t = q^4/\varepsilon\nu$ is set to be 66 in the case of the low Reynolds number while the numerical simulation of the high Reynolds number begins from $Re_t = 422$, where $q = (\overline{u_i u_i})^{1/2}$ and $\varepsilon = \nu\overline{(\partial u_i/\partial x_j)(\partial u_i/\partial x_j)}$. The direct numerical simulation is carried out with a pseudo-spectral code developed by Rogallo (1981) for a homogeneous turbulence. The remeshing of the grid system is used to avoid its distortion. The resultant alias error is removed by a combination of phase shift and truncation of high wavenumbers.

Characteristics of Flow Field

Time evolution of the shear-rate parameter S^* is shown in Fig. 1. The definition of S^* is given as

$$S^* = S\frac{q^2}{\varepsilon}. \tag{1}$$

In the turbulent channel flow, S^* becomes $5 \sim 30$ in the buffer region $10 \leq y^+ \leq 40$, while in the logarithmic region $y^+ \geq 40$, S^* is below 5 (see Lee et al., 1990). We continued the simulation to the time $St = 6.0$ in the low Reynolds number case, while $St = 12.0$ in the high Reynolds number case. At the end of each simulation when the turbulence structure will be discussed later in

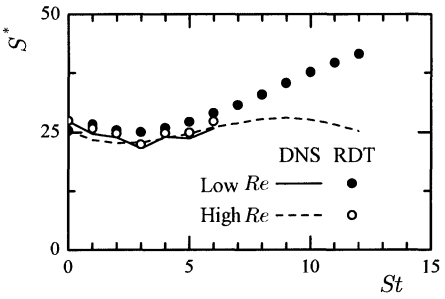

Figure 1. Time evolution of S^*.

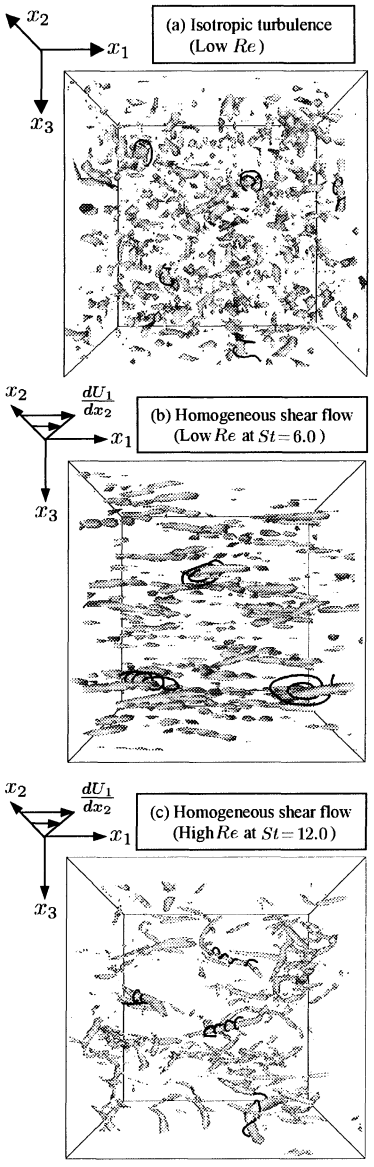

Figure 2. The isosurfaces of the second invariant of the deformation tensor and the streamlines around them. All figures show the half region in the streamwise direction.

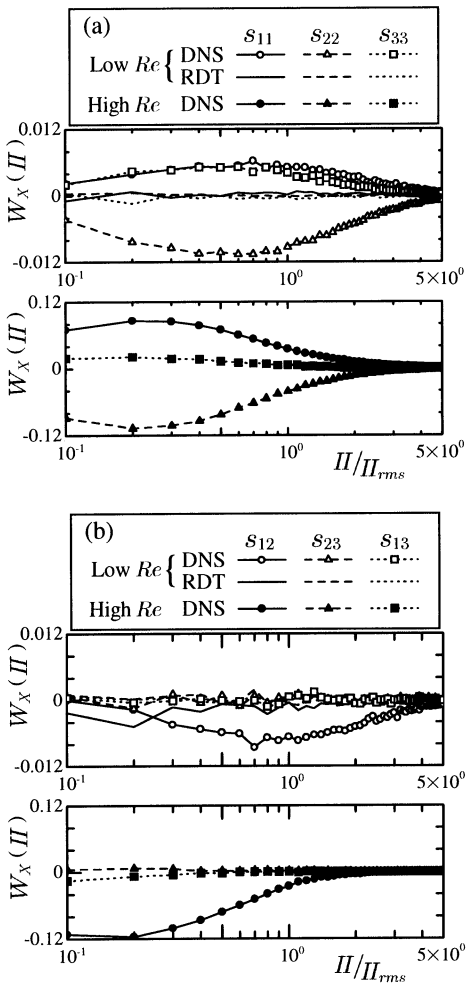

Figure 3. The expected value of s_{ij} versus II.

detail, S^* takes almost the same value in the buffer region where the quasi-streamwise vortices are frequently observed. It should be also mentioned that no significant difference is observed between DNS and RDT results in the low Reynolds number case. In the high Reynolds number case, on the other hand, marked differences do exist between DNS and RDT.

Figures 2 (a) and (b) show the isosurfaces of the second invariant of the deformation tensor II in isotropic turbulence and homogeneous shear flow at the low Reynolds number, respectively. The isosurfaces in the homogeneous shear flow at the high Reynolds number are shown in Fig. 2 (c). In all figures, the typical streamlines around the isosurfaces of II are plotted to show that they represent the vortical structures. It is assured that the blob-like vortical structures in isotropic turbulence are elongated in the streamwise direction to become the longitudinal vortices in a homogeneous shear flow. In the case of high Reynolds number, the same longitudinal vortices as observed in the case of low Reynolds number still exist, although much smaller scale structures are newly generated. The elongation of the vortical structures is still observed without the non-linear term, and hence is not due to the effects of the non-linear term(Kida and Tanaka, 1994).

Figure 3 shows the expected value of the strain rate tensor versus the second invariant of the deformation tensor. In the figure, $W_X(Y)$ is defined as follows:

$$W_X(Y) \equiv \int_{-\infty}^{\infty} XP(X,Y)dX\,, \tag{2}$$

where the parameter P is the p.d.f. of the variables X and Y, which represent s_{ij} and II in Fig. 3, respectively. One can note the marked differences between DNS and RDT in the distribution of all diagonal components $s_{\alpha\alpha}$ (no summation convention on Greek indices), and one off-diagonal component s_{12}. In the region $II > 0$ of DNS at the low Reynolds number, each component of the strain rate tensor is expected to satisfy the following relations:

$$s_{11},\ s_{33} > 0, \qquad s_{22},\ s_{12} < 0. \tag{3}$$

In RDT, all its components become almost zero. When the Reynolds number becomes larger, s_{11}, s_{22} and s_{12} increase markedly, although the Reynolds number effect is not observed in s_{33}, the value of which is much smaller than the other two diagonal components.

Kinematics of Vortical Structure

Next, we will discuss how the strain rate tensor affects the kinematics of the vortical structures detected by the positive II. Then, numerous vortical structures are educed by using the positive II in the low Reynolds number homogeneous shear flow at $St = 6$ (at $St = 12.0$ in the high Reynolds number flow), and conditionally averaged over the entire flow field to know the most expected effects of the strain rate tensor on the longitudinal vortices. The method of the conditional averaging is based on the procedures used in Jeong et al. (1997) and summarized as follows:
(1) Detect the local maximum of the second invariant II in the cross streamwise planes (positive II is used to identify the vortical structure, while ω_x is used to distinguish between structures with a different sense of the rotation), (2) Link the local maximum of II as the core of the longitudinal vortex, (3) Identify the individual longitudinal vortex if it satisfies the criterion that its streamwise length is larger than $(1/13)L_x$ in the low Reynolds number case and $(1/16)L_x$ in the high Reynolds number case, which approximate 42 $\sqrt{\nu/S}$ and 34 $\sqrt{\nu/S}$, respectively (the condition to capture the large scale longitudinal vortices), (4) Ensemble average the educed vortical structures with the sense of the rotation by aligning the mid-point of their streamwise extent. It should be noted that our method for detecting the vortex is not affected by a threshold value of II, although the vortical structures are excluded by

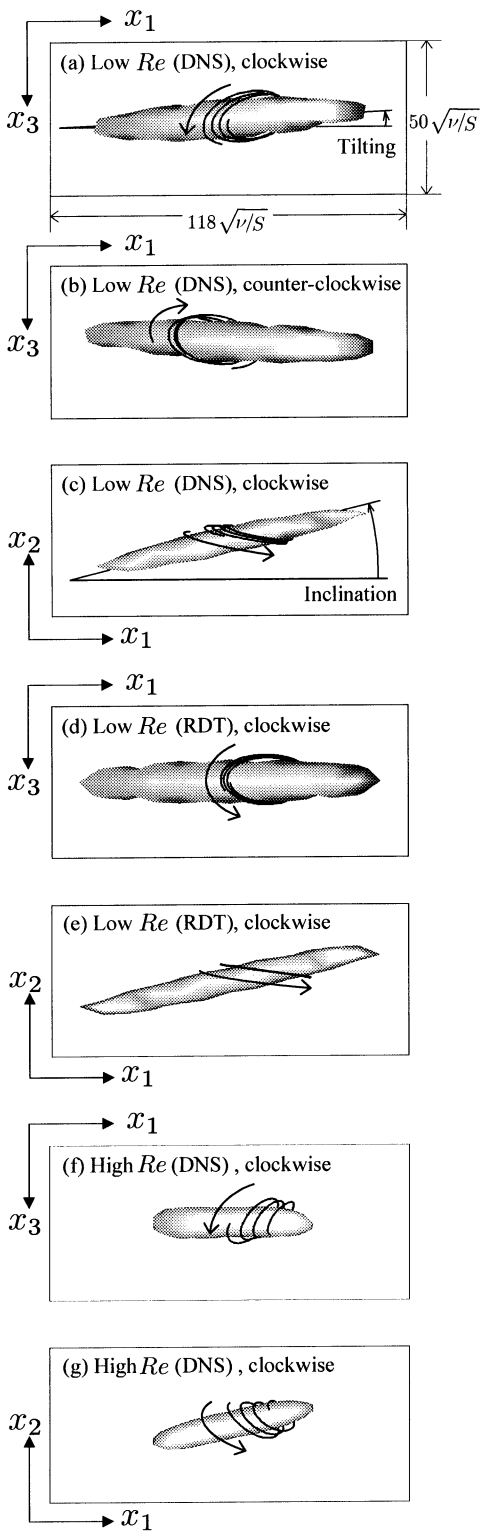

Figure 4. The isosurfaces of second invariant of the deformation tensor and the three-dimensional streamlines.

the streamwise length of the longitudinal vortex.

In all cases, the number of the educed vortical structures is approximately 400 (200 clockwise and 200 counter-clockwise vortices). Figures 4(a)-(g) show the conditionally averaged longitudinal vortices (Figs. 4(a)-(c) represent the vortical structure of DNS at the low Reynolds number seen from the different angles, while the RDT results are shown in Figs. 4(d) and (e). The results in the case of high Reynolds number are shown in Figs. 4(f) and (g)). The second invariant of the deformation tensor and streamlines are those calculated from the conditionally averaged velocity fields. In both results of high and low Reynolds numbers of DNS and RDT, the isosurfaces are elongated in the x_1-direction (streamwise direction), and the wrapping of streamlines around them is clearly observed. Hence, the non-linear term is not required to generate the elongated vortical structures, although a difference in the streamline does exist between DNS and RDT. The streamlines of DNS become spiral and stretched in the streamwise direction, indicating that the longitudinal vortex should be under the effects of the strain rate $\partial u_1/\partial x_1 > 0$, i.e., vortex stretching. The stretching of the streamline is more enhanced in the high Reynolds number case, which is consistent with the results of Fig. 3(a).

It is also found that in the $x_1 - x_3$ plane the averaged longitudinal vortices with the positive (negative) ω_x tend to tilt at a positive (negative) angle in the low Reynolds number case, while all of them slant at the positive angle in the $x_1 - x_2$ plane. The similar inclination and tilting of the longitudinal vortices are observed in a turbulent channel flow (Jeong et al., 1997). In the high Reynolds number case, the averaged longitudinal vortex has no tilting angle. This should be because the association between the rotational direction and the tilting angle will be lost although longitudinal vortices are tilted in the instantaneous flow field (see Fig. 2(c)).

Figure 5 shows the distribution of the streamwise velocity fluctuation in the cross streamwise plane, which clearly shows the mechanism how $s_{12} \sim (\partial u_1/\partial x_2)/2$ becomes negative in the vortical structures. It should be noted that the low speed fluid is lifted up to a vortex side by its rotational motion, while the high speed fluid is moved downward. Velocity fluctuations thus created are further transported and the vortex is wrapped by the fluid carrying velocity fluctuations u_1. This process makes $\partial u_1/\partial x_2$ largely negative in the vortex and is named wrapping (Jimenze and Moin, 1991; Guezennec et al., 1990). As seen from Fig. 5(c), the wrapping of the streamwise velocity fluctuation is more clearly observed in the case of high Reynolds number. Thus, $\partial u_1/\partial x_2$ should take a larger negative value (see Fig. 3(b)). The wrapping enhances the vortex stretching in the streamwise direction as illustrated in Fig. 6. Because the vortex has the positive inclination angle in the $x_1 - x_2$ plane, the positive strain rate ($\partial u_1/\partial x_1 > 0$) is generated in the process of the above-mentioned wrapping.

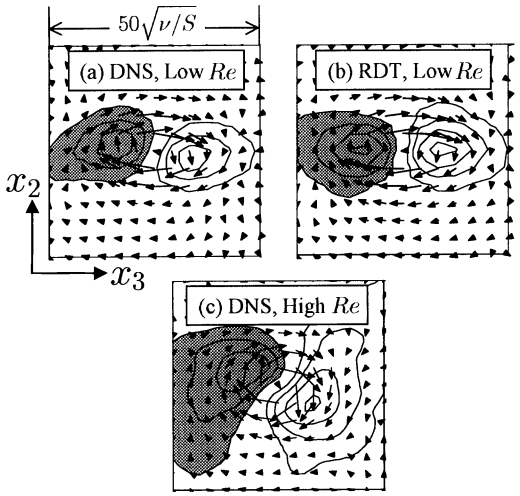

Figure 5. Velocity vectors and contours of u_1 in x_2-x_3 plane: The contour lines are plotted (a) from -4.0 to 4.0 with an increment of 1.0, (b) from -5.0 to 5.0 with an increment of 1.0 and (c) from -6.0 to 8.0 with an increment of 2.0. The shaded regions represent the negative value of u_1.

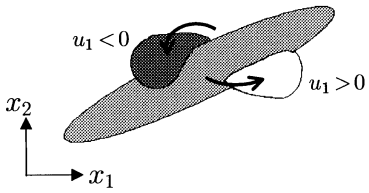

Figure 6. Schematics for the mechanisms of vortex stretching.

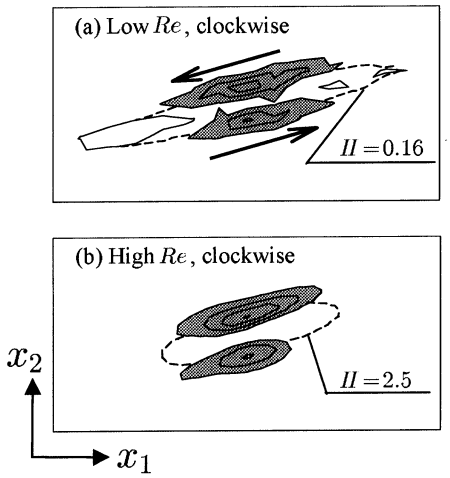

Figure 7. The contours of $-u_1u_2$ in x_1-x_2 plane. The contour lines are plotted (a) from -0.3 to 0.1 with an increment of 0.1, (b) from -8.0 to -2.0 with an increment of 2.0. The shaded regions represent the negative value of $-u_1u_2$. Both figures are the results of DNS.

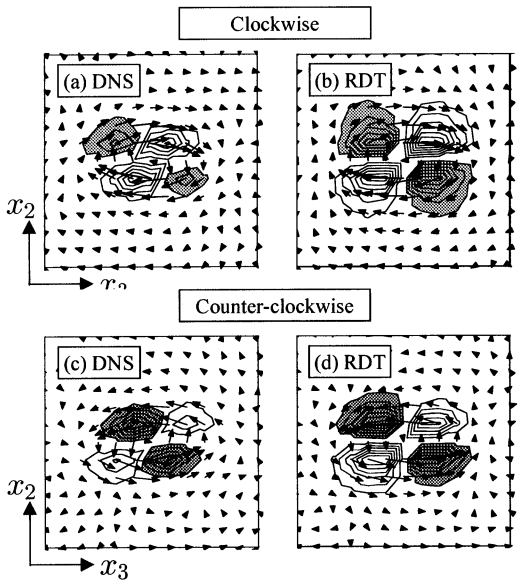

Figure 8. Velocity vectors and contours of $-u_2u_3$ in x_2-x_3 plane in the low Reynolds number case: The contour lines are plotted (a) from -0.75 to 1.25 with an increment of 0.25, (b),(d) from -0.6 to 0.6 with an increment of 0.1, (c) from -1.25 to 0.75 with an increment of 0.25. The shaded regions represent the negative value of $-u_2u_3$.

When the Reynolds number becomes larger, transferring of u_1 is so remarkable, and hence the vortex stretching is promoted. Figure 7 shows the instantaneous distribution of the Reynolds shear stress $-u_1u_2$ in the $x_1 - x_2$ plane. It is found that the wrapping of u_1 around the vortex contributes to the countergradient momentum transfer, and thus produces the intensive negative region of the Reynolds shear stress, i.e., $-u_1u_2 < 0$, in the upper right and the lower left of the streamwise vortex. When the Reynolds number becomes larger and the wrapping is more enhanced, $-u_1u_2$ takes a larger negative value. Thus generated Reynolds shear stress should contribute to $\partial u_2/\partial x_2 < 0$ as well as $\partial u_1/\partial x_1 > 0$, which is clearly observed statistically in Fig. 3(a).

Figures 8(a)-(d) show the instantaneous $-u_2u_3$ distribution in the low Reynolds number case. The result of RDT shows that the contours of $-u_2u_3$ show a cloverleaf pattern with alternative sign, so that the spatial averaged Reynolds stress $-u_2u_3$ should vanish. In contrast, the DNS result shows that $-u_2u_3$ is predominantly positive and negative for the clockwise and counter-clockwise vortices, respectively, which should be associated with the strain rates $\partial u_2/\partial x_2 < 0$ and $\partial u_3/\partial x_3 > 0$. Figure 9 shows the instantaneous $-u_2u_3$ distribution in the case of high Reynolds number. It is found that $-u_2u_3$ becomes nearly the same cloverleaf pattern as observed in RDT (Fig. 8). This should be because when the Reynolds number becomes larger, the

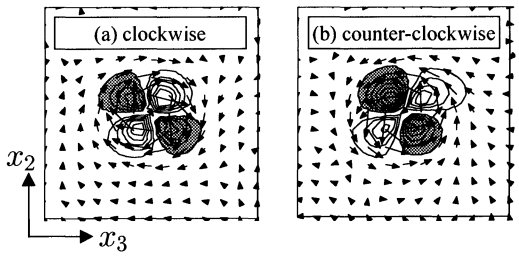

Figure 9. Velocity vectors and contours of $-u_2u_3$ in x_2-x_3 plane in the high Reynolds number case: The contour lines are plotted (a) from -20.0 to 30.0 with an increment of 5.0, (b) from -30.0 to 20.0 with an increment of 5.0. The shaded regions represent the negative value of $-u_2u_3$.

positive value of $\partial u_3/\partial x_3$ becomes negligible in comparison to the negative value of $\partial u_2/\partial x_2$, which is enhanced by the wrapping of u_1 around the streamwise vortex as discussed before (see Fig. 7).

CONCLUSIONS

Direct numerical simulations of homogeneous shear flows at relatively high and low Reynolds numbers are performed to investigate the kinematics of the longitudinal vortices which are objectively detected and conditionally averaged so as to obtain the most probable vortical structure. The results of DNS are compared with the RDT predictions to elucidate the effects of non-linear term. Moreover, the effects of Reynolds number are discussed. As a result, the following conclusions are established:

(1) In a homogeneous shear flow, the longitudinal vortices are generated. They are inclined in the $x_1 - x_2$ plane and tilted at a positive and negative angle in the $x_1 - x_3$ plane by the rotational direction of the vortex. The similar inclination and tilting of the longitudinal vortices are observed in a turbulent channel flow (Jeong et al., 1997). However, when the Reynolds number becomes larger, the association between the tilting angle and the rotational direction of the streamwise vortex is lost.

(2) With the non-linear term, the kinematics of the longitudinal vortex is affected by the strain rate tensor; the compression in the vertical direction ($s_{22} < 0$), the stretching in both the streamwise and spanwise directions and the shear stress $s_{12} < 0$. These strain rates are associated with the vortex stretching, the wrapping and generation of the Reynolds shear stresses as follows: The streamwise fluctuations generated at the sides of the streamwise vortex are wrapped around the vortex, in the course of which the strain rate, s_{12}, becomes negative and the vortex is stretched in the streamwise direction. The wrapping also contributes to the counter-gradient momentum transfer, i.e., $-u_1u_2 < 0$, which is associated with the strain rates $s_{11} > 0$ and $s_{22} < 0$. When the Reynolds number increases, the positive value of $\partial u_3/\partial x_3$ becomes negligible in comparison with other normal strain rates $\partial u_1/\partial x_1$ and $\partial u_2/\partial x_2$ which are enhanced by the wrapping of u_1 around the streamwise vortex.

ACNOWLEDGEMENT

This work was supported by the Ministry of Education, Science, Sports and Culture through Grants-in-Aid for both Scientific Research (B) (No. 10450085) and Encouragement of Young Scientists (No. 10750148).

REFERENCES

Guezennec, Y., Strech, D. and Kim, J., 1990, "The structure of turbulent channel flow with passive scalar transport," *Proc. Summer Program, Center for Turbulence Research, Stanford university*, pp. 127-138.

Iida, O. and Nagano, Y., 1998, "The relaminarization mechanisms of turbulent channel flow at low Reynolds numbers," *Flow, Turbulence and Combustion*, Vol. 60, pp. 193-213.

Jeong, J., Hussain, F., Schoppa, W. and Kim, J., 1997, "Coherent structures near the wall in a turbulent channel flow," *J. Fluid Mech.*, Vol. 332, pp. 185-214.

Jimenze, J. and Moin, P., 1991, "The minimal flow unit in near-wall turbulence," *J. Fluid Mech.*, Vol. 225, pp. 213-240.

Kida, S. and Tanaka, M., 1994, "Dynamics of vortical structures in a homogeneous shear flow," *J. Fluid Mech.*, Vol. 274, pp. 43-68.

Kline, S. J., Reynolds, W. C., Schraub, F. A., and Runstadler, P. W., 1967, "The structure of turbulent boundary layers," *J. Fluid Mech.*, Vol. 30, pp. 741-773.

Lee, M. J., Kim, J. and Moin, P., 1990, "Structure of turbulence at high shear rate," *J. Fluid Mech.*, Vol. 216, pp. 561-583.

Matsumoto, T., Nagano, Y. and Tsuji, T., 1994, "The effect of mean shear on homogeneous turbulence (Turbulence Statistics and Turbulence Models)," *Trans. JSME: Ser. B*, Vol. 60, pp. 1653-1660, in Japanese.

Robinson, S. K., 1991, "The kinematics of turbulent boundary layer structure," *NASA TM*-103859.

Rogallo, R. S., 1981, "Numerical experiments in homogeneous turbulence," *NASA TM*-81315.

Rogers, M. M. and Moin, P., 1987, "The structure of the vorticity field in homogeneous turbulent flows," *J. Fluid Mech.*, Vol. 176, pp. 33-66.